EJN fens European Journal of Neuroscience

European Journal of Neuroscience, Vol. 34, pp. 1310–1319, 2011 doi:10.1111/j.1460-9568.2011.07855.x

NEUROSYSTEMS

Regional quantification of developing human cortical shape with a three-dimensional surface-based magnetic resonance imaging analysis *in utero*

Hui-Hsin Hu,[1,2] Chih-I Hung,[1,2] Yu-Te Wu,[1,2,3] Hui-Yun Chen,[1,2] Jen-Chuen Hsieh[2,3] and Wan-Yuo Guo[4,5]
[1]Department of Biomedical Imaging and of Radiological Sciences, National Yang-Ming University, Taipei, Taiwan
[2]Integrated Brain Research Laboratory, Department of Medical Research and Education, Taipei Veterans General Hospital, Taipei, Taiwan
[3]Institute of Brain Science, National Yang-Ming University, Taipei, Taiwan
[4]Department of Radiology, Taipei Veterans General Hospital at 201, Section II, Shih-Pai Road, 11217 Taipei, Taiwan
[5]Faculty of Medicine, School of Medicine, National Yang-Ming University, Taipei, Taiwan

Keywords: cortical folding, fetus, growth pattern, gyrification, shape

Abstract

Although regional differences in cerebral volume have been revealed in developing human brains, little is known regarding the regionalization of cortical shape. This study documented the regional and quantitative shape difference of cortical surfaces for *in utero* normal fetal brains over a time period essential for the formation of primary cortical folding (22–33 weeks). Each brain surface with complete three-dimensional morphology was manually extracted from the reconstructed image, which combined surface information from three orthogonal magnetic resonance images *in utero*. An innovative parcellation was used to dissect the fetal brains into frontal, parietal, temporal and occipital lobes, and to avoid the determination of non-existent and immature sulci for young fetuses. Distinct cortical shapes were encoded by the shape index automatically. The results of this study show faster shape changes in the occipital lobe than in other regions. Both regional and global shape patterns show that the gyral surface smoothens, whereas the sulcal surface becomes more angular, with gestational age. In addition, the smoothing of gyri is related mainly to the changes in shape of gyral crowns. This study presents the regional differences in early gyrification from the novel aspect of shape. The results of shape pattern analysis for normal fetuses may act as a reference in assessments of prenatal brain pathology and in extensive comparisons between various life stages.

Introduction

In utero magnetic resonance (MR) images (MRIs) benefit investigation of the early gyrification of human fetal brains. Combined with the technique of brain image reconstruction, fetal MRIs can provide the complete three-dimensional (3D) morphology of normally developing brains (Rousseau *et al.*, 2006; Jiang *et al.*, 2007; Kim *et al.*, 2009). Recent studies analyzed the local differences in the morphology of the cerebral cortex on the basis of the reconstructed fetal MRIs, and discovered a regionally varying growth rate in the volumetry of the cortical sheet (Habas *et al.*, 2010a,b; Rajagopalan *et al.*, 2011) and in the thickness of a transient cortical laminar, subplate zone (Corbett-Detig *et al.*, 2011). This demonstrates that the regional differences in growth rate characterize the development of early gyrification.

The shaping of the sulci and gyri is an important process, as it relates to the mechanism that deforms the cerebral cortex (Van Essen, 1997; White *et al.*, 2010). Abnormal shape patterns of early gyrification have been described in certain cerebral developmental disorders, possibly resulting from the impairment of cellular maturation events (Dubois *et al.*, 2008b). As an example, microcephaly, which is defined as a cranial size below the third percentile, is probably caused by disturbed neuronal proliferation or excessive programmed cell death (Barkovich *et al.*, 1998), and presents as a simplified gyral pattern (Garel, 2004). That is, the gyral shape tends to be wide and shallow as compared with normal controls at the same age (Garel, 2004). Therefore, reliable quantification of the normal shape pattern may assist in the assessment of abnormal brains during intrauterine life, and may provide insights into neurodevelopmental disorders.

This study was aimed at modeling the regional shape differences with respect to early gyrification through an MRI-based surface analysis of a series of normal fetal brains *in utero*. To achieve this, we proposed a new parcellation of fetal brains and utilized a reliable measurement that discriminates cortical surface shapes. Also, the current study focused especially on the shape geometry of primary cortical folding, which appears in the earliest stage and sustains deformation with age (22–33 weeks). As shown in Fig. 1, the Sylvian fissure (black arrows) deforms dramatically with increasing gestational

Correspondence: Wan-Yuo Guo, [4]Department of Radiology, as above.
E-mail: wyguo@vghtpe.gov.tw

Received 22 December 2010, revised 22 July 2011, accepted 28 July 2011

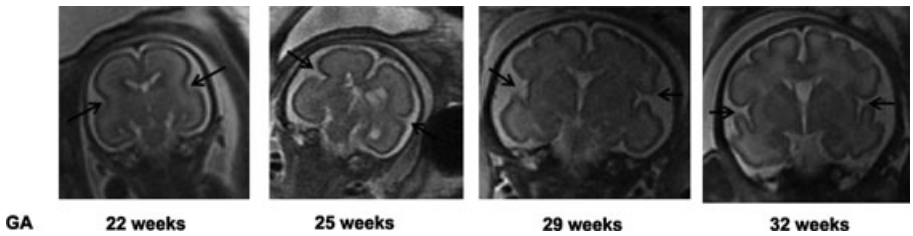

FIG. 1. A chronological series of original coronal brain images. The shape of the Sylvian fissure (black arrow) keeps deforming with increasing GA.

age (GA). It is of note that ultrafast *in utero* MRI acquisition sequences, which reduce the possibility of fetal movement artefacts during scanning without sedation, require large slice thicknesses (4 or 5 mm) to preserve a sufficient signal-to-noise ratio for the small volume of fetal brains. Therefore, the clinically acquired MRI exhibits better in-plane resolution (Fig. 2, first plot in row A) but poorer resolution in terms of slice thickness (Fig. 2, second and third plots in row A). To solve this problem, this experiment required the adoption of a technique of brain reconstruction for fetal MRIs (Rousseau *et al.*, 2006), extracting the cortical shapes from the reconstructed images that provided complete 3D surface information.

Materials and methods

Subjects

This study analyzed the MRIs of 27 normal fetal brains between 22 and 33 weeks of gestation. Each fetus was from a single pregnancy. We used fetuses that had been examined for non-central nervous system (CNS) abnormalities. The fetuses had undergone an additional MR examination of the brain and/or had shown suspicious ventricular dilatation on ultrasound, but were regarded as normal fetuses upon further MR examination. The Institute Review Board of Taipei Veterans General Hospital (VGHIRB No. 96-12-26A) approved this study, and informed consent for MR examination was obtained from each mother.

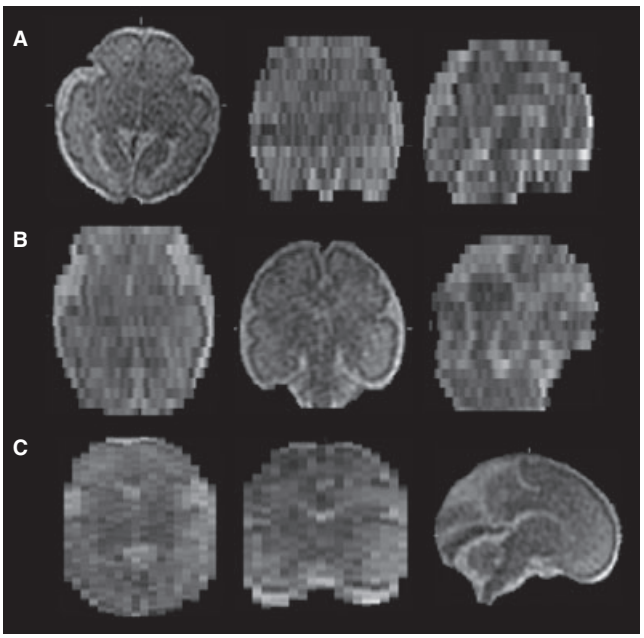

FIG. 2. Three orthogonal brain images from a 29-week fetal brain. Rows A, B and, C are the axial, coronal and sagittal MR images, respectively, with a resolution of $1 \times 1 \times 5$ mm^3. Columns from left to right display an image separately from three viewing angles, i.e. axial, coronal and sagittal views. The original fetal MR brain images *in utero* present excellent in-plane resolution but lose 3D coherence.

Neuroimaging

The scanning sequence was half-Fourier acquisition single-shot fast spin-echo (SSFSE from GE, Milwaukee, WI, USA; or HASTE from Siemens, Erlangen, Germany) with body phase-arrayed coils. The system used was a 1.5-T MR scanner (GE or Siemens). The echo time was 95 ms, and the repetition time was 11.9 ms. The overall scanning time, including maternal positioning, was usually ~20 min. Three orthogonal image views of the fetal brain (coronal, axial and sagittal planes) were acquired. To reduce the effect of inter-series fetal motion and to ensure standard orthogonal brain imaging, the image series that had just been obtained was employed as the direct scout for the subsequent series. If the fetal brain was not perpendicular to the axis of the magnet, double-oblique or triple-oblique plane selection was necessary to obtain standard orthogonal views. All scans were reviewed by the same experienced neuroradiologist (W.Y.G.).

The slice thickness was 4 or 5 mm, for preservation of a sufficient signal-to-noise ratio and reduction of fetal movement during ultrafast MR imaging. Of 27 fetuses, seven cases were scanned with a slice thickness of 4 mm and 20 cases with a slice thickness of 5 mm. The GAs of the 4-mm cases were 167, 170, 190, 193, 197, 204 and 232 days; those of the 5-mm cases were 154, 159, 162, 163 165, 175, 182, 188, 191, 193, 208, 210, 211, 211, 212, 218, 222, 225, 231 and 234 days. The GA difference between the 4-mm and 5-mm groups was statistically insignificant (two-sample t-test: $t = -0.1796$, $P = 0.8601$). Two matrix sizes, 256×256 and 512×512, were obtained with two fields of view, 280×280 or 400×400 mm^2, respectively. Image resolutions were 1.09×1.09 mm^2 or 0.78×0.78 mm^2. To obtain consistent in-plane resolution between different images, each MR slice was re-sampled to 1×1 mm^2 by linearly interpolating the image intensity without losing or adding detailed cerebral contour features. When this was done, the image resolution became $1 \times 1 \times 4$ or $1 \times 1 \times 5$ mm^3.

Reconstruction of fetal brain image with 3D coherence

The super-resolution technique of 3D fetal brain reconstruction (Rousseau *et al.*, 2006) was implemented in this study to obtain the image with 3D coherence that could be used for *in utero* surface-based analysis. Normalized mutual information (NMI), an intensity-based similarity measure, was used to coregister three orthogonal MRIs (coronal, axial and sagittal planes) for the fetuses. The NMI reaches a maximum when the two slices or two images are optimally aligned. Fetal motion was modeled as a 3D rigid body transformation, and was

corrected with two-level image registration – 3D-to-3D image registration and the 2D slice to 3D image registration. Each image, together with each slice within an image, was separately coregistered, and the images were superimposed on each other iteratively until the NMI maximum was achieved. The programming language used was MATLAB7.0 (MathWorks, Natick, MA, USA). The resolution of the resultant brain images with 3D coherence became $1 \times 1 \times 1$ mm^3. Figures 2 and 3 show the three original images and a 3D reconstructed image for a 29-week fetus.

Fetal brain image extraction

The fetal brain image was manually extracted from the volumetric data with 3D coherence. The contour between cerebrospinal fluid and the cerebral cortex, excluding the cerebellum and the spine, was traced with the free software MIPAV (Center for Information Technology, National Institutes of Health), which provided a user interface and semi-automatic methods for facilitating brain segmentation. The intra-rater error was 3% for one rater, and the inter-rater error was 8% for two independent raters. Accordingly, only a single rater (H.H.H.) segmented all brain images. An example of brain image extraction is shown in Fig. 3, where the rater simultaneously inspected three orthogonal views (Fig. 3B) to ensure the topological correctness of the brain contours. This was necessary because sulci orientations often allow them to be identified only from one viewing angle. Brain contours were finally delineated via the coronal view (Fig. 3A). The delineation of brain contours for a volumetric image took 2–5 h.

Figure 4 shows an example of the fetal brain surface created separately from coronal, axial, sagittal and reconstructed images (from left to right panel) at the 29th week of gestation. The brain surfaces created from the original fetal brain images showed obvious 'gap' artefacts (white arrows in Fig. 4) in the blue area, because of insufficient resolution resulting from slice thickness. No 'gap' artefact appeared in the reconstructed brain surface (the rightmost panel in Fig. 4), suggesting that the reconstructed image can provide sufficient surface information to improve the 3D topological accuracy for the fetal brain surface.

Fetal brain parcellation

To avoid the determination of non-existent and/or immature gyri/sulci for young fetuses, our previous work focused on the anterio-posterior development of fetal brains, and partitioned the original coronal images by three slices that located pivotal anatomical landmarks. Extending this framework to reconstructed images, the current study involved parceling fetal brains in three dimensions and selecting four slices that located the central sulcus, the sylvian sulcus, the anteriority of the temporal lobe, and the posterior endpoint of the lateral horns. These anatomical landmarks were verified separately from three orthogonal views, owing to the complete brain topology provided by the reconstructed image (Fig. 4).

The four slices were selected for brain parcellation as follows (Fig. 5): (i) the coronal image (1C) that located the central sulcus was used for distinguishing between the frontal and parietal lobes – this slice was determined by the location of the central sulcus on the midsagittal plane (the red line in 1B), based on the position of the central sulcus in the adult brain on the Talairach grid (the E2 block in 1A); (ii) the axial image (2B) that located the Sylvian sulcus was used for delimiting the temporal lobe beneath the frontal and parietal lobes – this slice was determined by the position of the Sylvian sulcus on the coronal slice (green line in 2A); (iii) the coronal slice (3B) located the anteriority of the temporal lobe – the sagittal slice (the cross in 3A) also confirmed the anteriority of the temporal lobe (the cross in 3B); and (iv) the coronal slice (4B) located the posterior endpoint of the

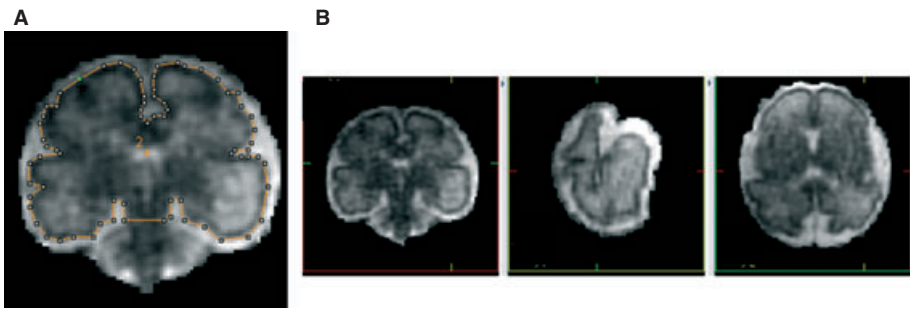

FIG. 3. A typical example of brain extraction from the reconstructed image of a 29-week fetus. (A) The brain contour between the fetal cortex and cerebrospinal fluid was manually traced via the coronal view. (B) The three orthogonal views, coronal, sagittal, and axial (from left to right), were simultaneously inspected for acquistion of accurate brain contours. As compared with the original brain images in Fig. 2, the reconstructed image shows excellent 3D coherence.

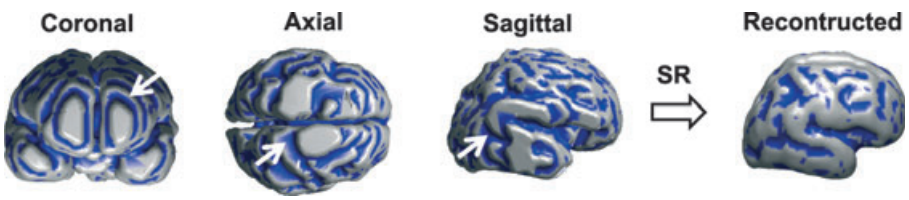

FIG. 4. Brain surface rendering from original and reconstructed images of a 29-week fetus. From left to right, each panel corresponds to fetal brain surfaces created from the original coronal, axial, sagittal and reconstructed 3D coherent images. The gray area with a positive SI value represents the gyral surface, and the blue area with a negative SI value represents the sulcal surface. The white arrows indicate the area with a 'gap' artefact derived from the large slice thickness of the original fetal MR brain images (5 mm in this case). Such a 'gap' artefact is corrected in the reconstructed 3D coherent brain images. SR, super-resolution reconstruction.

lateral horns, and was used for distinguishing the occipital lobe from the temporal and parietal lobes – this slice was chosen because neonatal brain images that had been transformed into the Talairach atlas (Gilmore *et al.*, 2007) demonstrated that the occipital region ranged from the posterior endpoint of the lateral horns to the occipital pole (Fig. 1D in Gilmore *et al.*, 2007).

As shown in the top right panel of Fig. 5, these four slices dissected the fetal brain into frontal, temporal, parietal and occipital lobes.

Quantification of cortical surface shape by shape index (SI)

This study employed the SI to parameterize the growth pattern of cortical shapes between distinct brain lobes.

Definition of the SI

The SI quantifies the surface shape surrounding a 3D point, and is given by (Koenderink & van Doorn, 1992).

$$\text{Shape index (SI)} = \frac{2}{\pi}\arctan\frac{k_2 + k_1}{k_2 - k_1} \quad (k_1 \geq k_2),$$

where k_1 and k_2 are the maximum and minimum principal curvatures of a surface point, respectively. The SI satisfies an evident truth – all of the spheres may differ in size, although they retain the same shape. As illustrated in Fig. 6, two points (p and p') on the cylindrical surfaces ($k_1 = k_1' = 0$, $k_2 < 0$, $k_2' < 0$) with unequal radii ($r > r'$) show the same SI value:

$$\frac{2}{\pi}\arctan\left(\frac{k_2+0}{k_2-0}\right) = \frac{2}{\pi}\arctan\left(\frac{k_2'+0}{k_2'-0}\right) = 0.5$$

That is, regardless of the size of the object, the SI is related only to the surface shape.

Being the inverse tangent normalized by $2/\pi$, the SI is a series of continuous values within the range of $[-1, 1]$, corresponding to transitional shapes between concavity and convexity. Figure 7 shows several SI values and the corresponding definite shapes, such as the spherical ($|SI| = 1$), cylindrical ($|SI| = 0.5$) and saddle-like ($|SI| < 0.5$) surfaces (for more details on the shapes in Fig. 7, see the Appendix). A surface point on a flat plane ($k_1 = k_2 = 0$) and a transition point between the concavity and convexity ($k_1 = -k_2$, the 'saddle' in Fig. 7) both have SI = 0. The higher the absolute SI value, the more angular is the surface shape. The lower the absolute SI value, the smoother is the surface shape.

Calculation of SI

The SI was calculated from the gradient of the image intensity, on the basis of the method proposed by Thirion & Gourdon (1993). This method avoids a parametric model on the image iso-surface. To eliminate the possibility of inconsistent intensity among images, which can lead to non-comparable results among subjects, we binarized image intensity prior to the SI calculation by assigning a value of 100 to the inside of the brain contour and a value of 0 to the background. We pinpointed the SI values on the surface voxels, all of which comprised a digital 3D iso-surface in an image.

The following describes the steps used to acquire the SI values on the surface voxels.

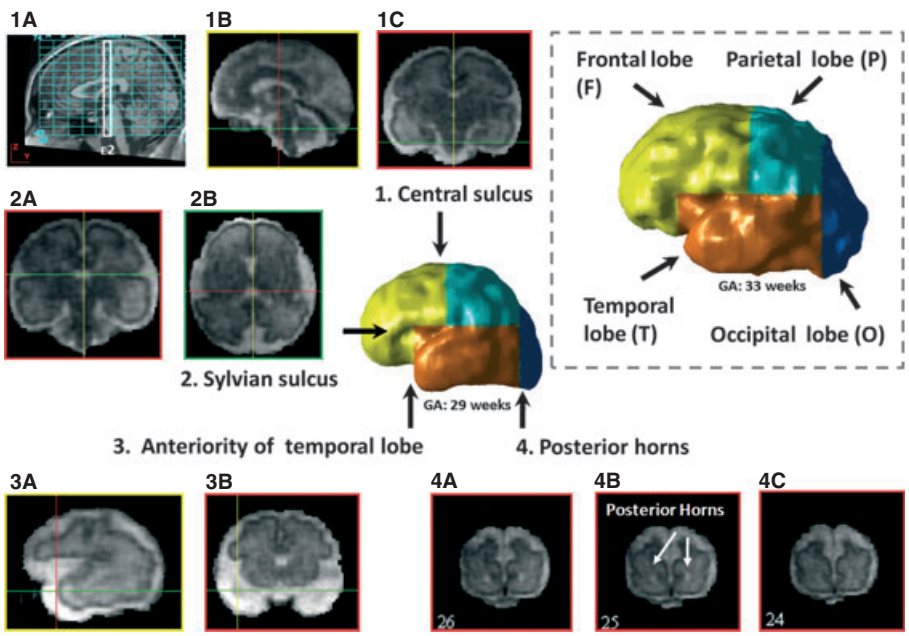

FIG. 5. Examples of four-lobe brain parcellation using reconstructed 3D coherent images for the 29-week and 33-week fetuses. Three coronal slices (1C, 3B, and 4B) together with one axial slice (2B) are used to divide the fetal brain into four lobes, including the frontal, parietal, temporal and occipital lobes (see the top right panel). These slices were selected on the premise of the Talairach grid and ventricular system. The slices from 1A to 1C determine the location of the central sulcus; 2A and 2B determine the location of the sylvian sulcus; 3A and 3B determine the anteriority of the temporal lobe; 4A to 4C determine the endpoint of posterior horns (4B) for the lateral ventricles. The outer edge of each slice is red, green, or yellow, corresponding to the coronal, axial or sagittal view, respectively. The cross in slices from one viewing angle represents the corresponding locations of the other two viewing angles. 1A displays the midsagittal plane of an adult brain, which is superimposed with the Talairach grids (refer to Hu *et al.*, 2009). The E2 block of the Talairach grid (1A) constitutes the main area of the central sulcus.

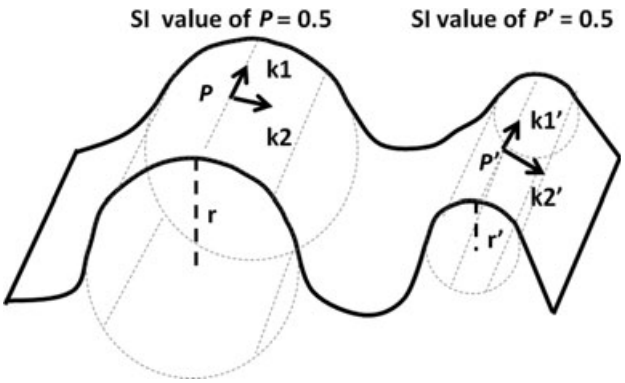

FIG. 6. Identical SI values between two points on cylindrical surfaces with unequal radii. The outward cylindrical surfaces represent the zero maximum ($k_1 = k_1' = 0$) and negative minimum ($k_2 < 0$, $k_2' < 0$) principal curvatures. Although p and p' are on the cylindrical surfaces with unequal radii ($r > r'$), these two points show the same SI value on the basis of the SI equation: $\mathrm{SI} = \frac{2}{\pi}\arctan(\frac{k_2+0}{k_2-0}) = \frac{2}{\pi}\arctan(\frac{k_2'+0}{k_2'-0}) = 0.5$ This demonstrates that all cylindrical surfaces may differ in size, but have the same shape.

First, let a digital 3D image be denoted by $f(x,y,z)$, and the partial derivatives, for simplicity, be denoted as follows: $\partial f(x,y,z)/\partial x$ by f_x, $\partial f(x,y,z)/\partial y$ by f_y, $\partial f(x,y,z)/\partial z$ by f_z, $\partial^2 f(x,y,z)/\partial x^2$ by f_{xx}, $\partial^2 f(x,y,z)/\partial y^2$ by f_{yy}, $\partial^2 f(x,y,z)/\partial z^2$ by f_{zz}, $\partial^2 f(x,y,z)/\partial x \partial y$ by f_{xy}, $\partial^2 f(x,y,z)/\partial y \partial z$ by f_{yz}, and $\partial^2 f(x,y,z)/\partial x \partial z$ by f_{xz}. These partial derivatives represent the intensity gradient among adjacent voxels. The mean curvature (S) and Gaussian curvature (K) at a voxel location (x,y,z) were as given by Thirion & Gourdon, 1993:

$$S = \frac{1}{2h^{3/2}}\left[f_x^2(f_{yy}+f_{zz}) - 2f_yf_zf_{yz} + f_y^2(f_{xx}+f_{zz}) - 2f_xf_zf_{xz} + f_z^2(f_{xx}+f_{yy}) - 2f_xf_yf_{xy}\right]$$

$$K = \frac{1}{h^2}\Big[f_x^2(f_{yy}f_{zz}-f_{yz}^2) + 2f_yf_z(f_{xz}f_{xy}-f_{xx}f_{yz}) + f_y^2(f_{xx}f_{zz}-f_{xz}^2) + 2f_xf_z(f_{yz}f_{xy}-f_{yy}f_{xz}) + f_z^2(f_{xx}f_{yy}-f_{xy}^2) + 2f_xf_y(f_{xz}f_{yz}-f_{zz}f_{xy})\Big],$$

where $h = f_x^2 + f_y^2 + f_z^2$.

The principal curvatures ($k_1$and k_2) at the location (x,y,z) on the images are the solutions of the following equation of the order two (Thirion & Gourdon, 1993):

$k_i(x,y,z) = S \pm \sqrt{\Delta}$, with $\Delta = S^2 - K$ (i = 1,2 and $k_1 \geq k_2$)

Finally, the SI values were acquired on the surface voxels by inserting the k_1 and k_2 values into the SI equation.

Statistical analysis

This study assessed the shape growth pattern of fetal gyrification both globally and regionally. The positive and negative SI values were used to specify the gyral and sulcal surfaces, respectively. The positive SI average was therefore termed a gyral SI, and the negative SI average was termed a sulcal SI. The global shape pattern was tested by using both the gyral SI and sulcal SI over the entire brain. The regional shape patterns were similarly tested by the gyral SI and sulcal SI across the four brain lobes (frontal, parietal, temporal and occipital regions). To facilitate comparison of the shape growth trend between sulci and gyri, the resultant SI-related measures were transformed into absolute values.

To better understand the distribution of SI values at particular GAs, the absolute frequencies of continuous SI values were also computed.

In addition, this study evaluated the growth pattern of brain folding based on the nine scales that demarcate continuous SI values (Table 1) (Koenderink & van Doorn, 1992). The SI values in Fig. 7 and the corresponding shapes determine the midpoint or the endpoint within each scale and their respective names. This enables us to imagine the shape of a given SI value. For example, the shape of SI = 0.9066 should be similar to a 'spherical dome' (Table 1; Fig. 7). On the basis of Table 1, the current study regrouped the neighboring SI values (e.g. SI = −0.997 and SI = −0.998) together, because they corresponded to almost the same shapes. The correlation between SI and GA for each scale (Table 1) was used to examine whether the shape pattern of fetal

TABLE 1. Nine-scale partition of SI

Local shape	Index range
Spherical cup	SI [–1, −0.875)
Trough	SI [−0.875, −0.625)
Rut	SI [−0.625, −0.375)
Saddle rut	SI [−0.375, −0.125)
Saddle	SI [−0.125, 0.125)
Saddle ridge	SI [0.125, 0.375)
Ridge	SI [0.375, 0.625)
Dome	SI [0.625, 0.875)
Spherical dome	SI [0.875, 1)

Courtesy of Koenderink & van Doorn (1992).
), open end of interval; [, closed end of interval.

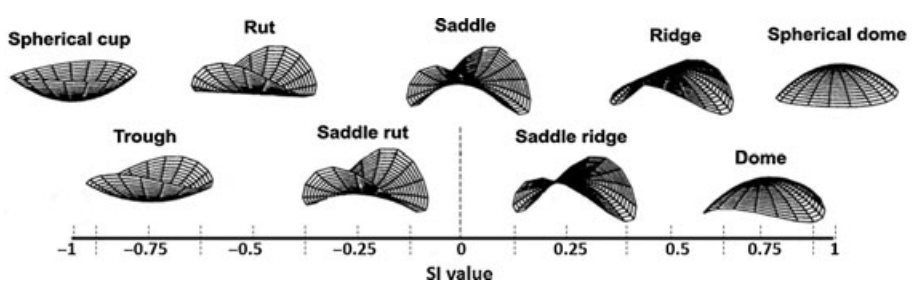

FIG. 7. SI values with the corresponding local shapes (courtesy of Koenderink & van Doorn, 1992). These local shapes exhibit definite relationships between maximum (k_1) and minimum (k_2) principal curvatures of a surface point (see the Appendix). These nine shapes determine either the midpoints or the endpoints of the scales in Table 1. The interval between any two dashed lines is equal to 1/8 of the total length 2.

gyrification is highly related to changes around any definite surface shapes, as illustrated in Fig. 7.

The line of best fit and the Pearson correlation coefficient (R) were used to evaluate the relationship between the SI value and GA. ANCOVA was used to test whether the linear growth rates vary from lobe to lobe. A multiple comparison procedure was adopted to determine where the differences that appeared by ANCOVA reached significance. All statistics were calculated with the MATLAB statistical toolbox (MathWorks), and the level of significance was set at 0.05.

Results

Of the 27 fetal brains subjected to *in utero* MR examination in this study, only two were excluded, because of the failure to reconstruct a coherent 3D image. The two excluded cases were at 193 and 208 days of gestation, with a slice thickness of 5 mm.

Surface shape encoding by SI

Figure 8 shows the 3D shape geometry of the fetal brain at different developmental stages. In Fig. 8, the cortical surface shapes were regrouped into the nine scales based on Table 1, and each SI scale was assigned a specific color. This facilitates visual inspection of the distribution of local surface shapes (Koenderink & van Doorn, 1992). The results show that the use of SI successfully quantifies the distinct 3D surface shapes of fetal gyrification, and that such geometrical features (shape) are analogous to anatomical ones (Fig. 8).

Global shape patterns between sulci and gyri

Figure 9 shows that the gyral SI significantly decreased with GA (left panel – $R = -0.89$, $P < 0.00001$), whereas the sulcal SI significantly increased with GA (right panel – $R = 0.9$, $P < 0.00001$). These results suggest that the gyral surface became smooth, whereas the sulcal surface became angular, over the development period for primary cortical folding (from 22 to 33 weeks).

The best-fit models of the SI values vs. GA (per day) were:
gyral SI = 0.7579 – 0.00113 × age
and
gyral SI = 0.1706 + 0.0011 ×age

Most of the normative data were within 95% of the confidence intervals (dashed lines in Fig. 9). The rate of smoothing of the gyral surface was close to that of the angulation of the sulcal surface.

Regional shape patterns across four brain lobes

Table 2 shows that all correlation coefficients between gyral SI and GA were significantly negative and that those between sulcal SI and GA were significantly positive. These results indicate that all brain

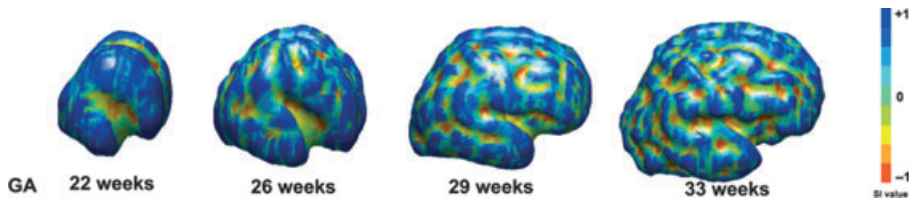

FIG. 8. Three-dimensional cortical shape geometry encoded by the SI. Four fetal brains at 22, 26, 29 and 33 weeks of gestation are separately displayed from left to right. The SI value is divided into nine scales on the basis of Table 1. The color bar displays the specific colors corresponding to nine scales.

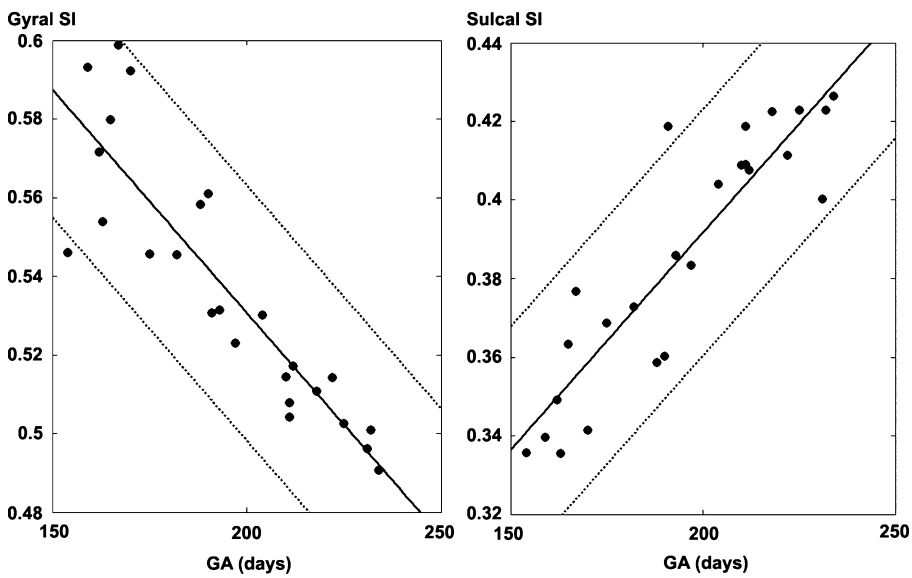

FIG. 9. Global shape patterns between sulcal and gyral surfaces. The gyral SI is defined as the positive SI averages, and the sulcal SI is defined as the negative SI averages. A significant decrease in the gyral SI with GA ($R = -0.89$, $P < 0.00001$) indicates that the gyral surface becomes smoother, whereas a significant increase in the sulcal SI ($R = 0.9$, $P < 0.00001$) indicates that the sulcal surface becomes more angular. Solid lines – the best fit of data. Dashed lines – the 95% confidence intervals of data.

TABLE 2. Regional shape growth rates and correlation coefficients (R) between SI and GA across four brain lobes

	O	P	F	T
Rate				
Gyral SI	−0.0015	−0.0006	−0.0009	−0.0005
Sulcal SI	0.0025	0.0011	0.0011	0.001
R				
Gyral SI	−0.76	−0.63	−0.74	−0.64
Sulcal SI	0.85	0.77	0.79	0.8

Unit of rate – SI value/day. All correlation coefficients approach significance with $P < 0.0009$. O, occipital; P, parietal; F, frontal; T, temporal.

lobes (Fig. 10) followed a trend identical to that of the global shape pattern (Fig. 9).

Additionally, both gyral SI and sulcal SI demonstrated a faster growth rate in the occipital lobe than in other areas (Table 2). The results of ANCOVA showed that the decreasing rate of gyral SI in the occipital lobe was significantly higher than those those in the parietal and temporal lobes (ANCOVA – $F_3 = 5.96$, $P = 0.0009$). No significant rate difference in gyral SI was found between the occipital and frontal lobes ($P > 0.05$). Similarly, the increasing rate of sulcal SI in the occipital lobe was significantly higher than those in the frontal, parietal and temporal lobes (ANCOVA – $F_3 = 9.42$, $P < 0.00001$).

Absolute SI frequencies at particular GAs

Both the global (Fig. 9) and regional (Fig. 10) growth patterns revealed smoothing of the gyral surface and angulation of the sulcal surface from 22 to 33 weeks of gestation. To examine whether such a shape pattern may correlate with the alterations in certain SI values, we inspected the absolute SI frequencies from the youngest to the oldest fetus (Fig. 11).

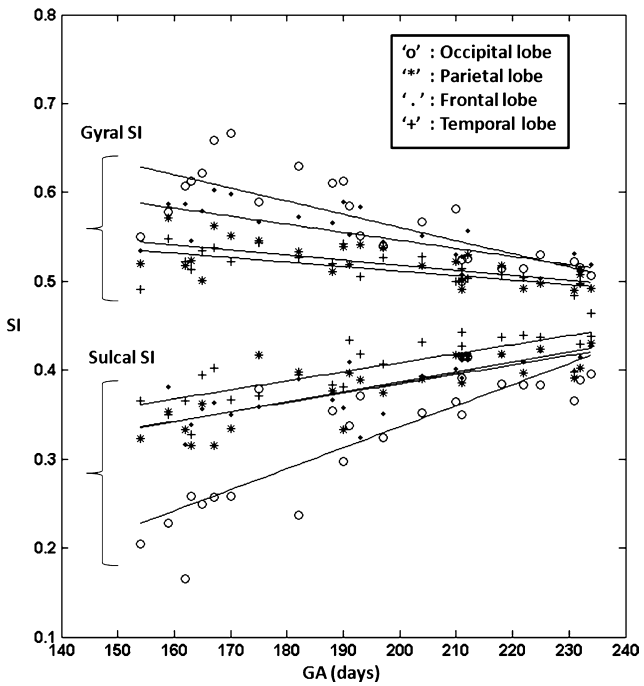

FIG. 10. Regional shape patterns across four brain lobes. The regional shape growth rates and correlation coefficients between SI value and GA are shown in Table 2. The results of ANCOVA (gyral SI, $F_3 = 9.42$, $P < 0.00001$; sulcal SI, $F_3 = 5.96$, $P = 0.0009$.) show that the occipital lobe changes faster than the other areas. O, occipital; P, parietal; F, frontal; T, temporal.

In Fig. 11, the absolute SI frequency reaches its peak around the convexities (SI ≥ 0.5) for younger fetuses and tends to distribute uniformly with increasing GA. That is, the SI frequencies of convexities appear to decrease with increasing GA. This implies that the smoothing of the gyral surface is highly correlated with the changes in the shape of gyral crowns.

Correlation between SI and GA for nine shape scales

We also used the nine shape scales (Table 1) to test whether the changes in the shape of the gyral crown reached statistical significance.

Our results revealed that the ridge and dome showed decreasing SI values with GA (ridge, $R = -0.76$, $P < 0.0001$; dome, $R = -0.83$, $P < 0.0001$) (Fig. 12), suggesting that the changes in shape of the gyral crown significantly varied with GA. In addition, the saddle rut significantly increased in SI value with GA ($R = 0.69$, $P = 0.0002$). Other shape scales showed insignificant correlations between the SI value and GA ($P > 0.05$).

Discussion

This *in utero* MRI-based study shows the global and regional patterns of early gyrification from the novel perspective of shape. Combining a new parcellation of fetal brains with an automatic quantification of cortical shapes, this study discovered that the regional shape pattern is congruous with the global pattern during the formation of primary cortical folding. The gyral surface becomes smoother with age, whereas the sulcal surface becomes more angular. Furthermore, the smoothing of gyri is highly correlated with changes in shape of gyral crowns. A significantly higher growth rate is found in the occipital lobe, revealing the regional difference in growth rate in the evolution of cortical surface shape for human fetal brains.

Both the regionalization and the shaping of the human cerebral cortex proceed from intrauterine life to the developmental stages after birth. During the first months after birth, normal neonates exhibit faster volumetric development in the occipital regions than in the prefrontal region, which may relate to more rapid maturation of the visual systems than prefrontal executive functions after birth (Gilmore *et al.*, 2007). In childhood and adolescence, the extensive synaptic pruning releases the tensile force of axonal connections and then alters the shape pattern of sulci and gyri. This includes the widening of sulcal fundi and a sharpening of gyral crowns (Van Essen, 1997; White *et al.*, 2003). In this study, normally developing brains show the regional differences in the shaping of cortical surface in the fetal stage. Such results may provide a useful baseline for the longitudinal regional shape analysis from the fetal stage to childhood and adolescence.

The finding of the most rapid sulcal shape change in the occipital lobe (22–33 weeks) (Fig. 10) is consistent with the voxel-based volumetric pattern, with more volume increases in the cortical sheet of occipital areas (20–28 weeks) (Rajagopalan *et al.*, 2011). This suggests that the shaping of the cortical surface may develop synchronously with the volumetric increment of the cortical layer in certain brain areas (e.g. the occipital lobe).

The shape changes of fetal brains have recently been investigated via the deformation displacement between the brain images and a voxel-wise template for young fetuses (Habas *et al.*, 2010a,b). Such a shape change appears mainly in the frontal lobe at 20–24 weeks (Habas *et al.*, 2010a). Nevertheless, the amount of displacement may

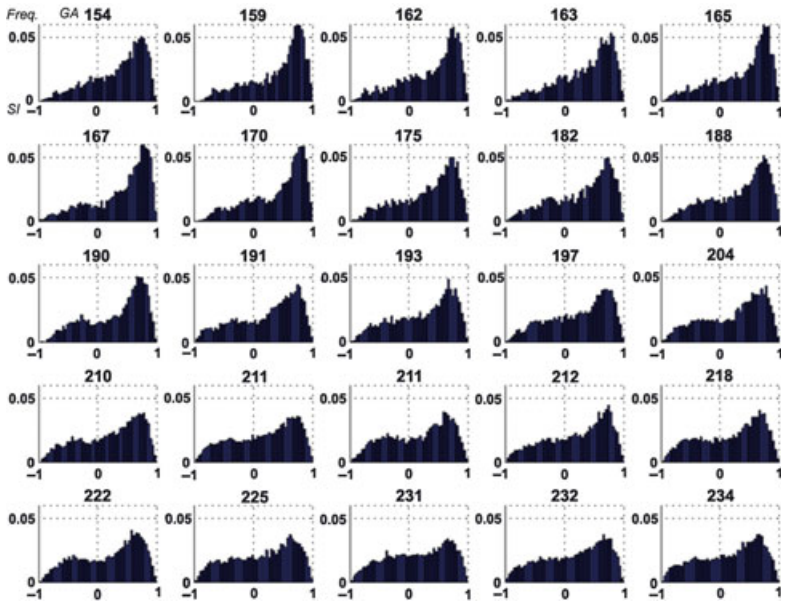

FIG. 11. Distribution of absolute SI frequencies at particular GAs. The absolute SI frequencies of 25 fetuses are shown from the youngest (the top left panel) to the oldest (the bottom right panel). The title of each panel indicates the fetal age, in days. The horizontal axis of each panel indicates the continuous SI values, and the vertical axis indicates the corresponding absolute frequencies. The absolute frequencies of the convexities (SI ≥ 0.5) apparently change with increasing GA.

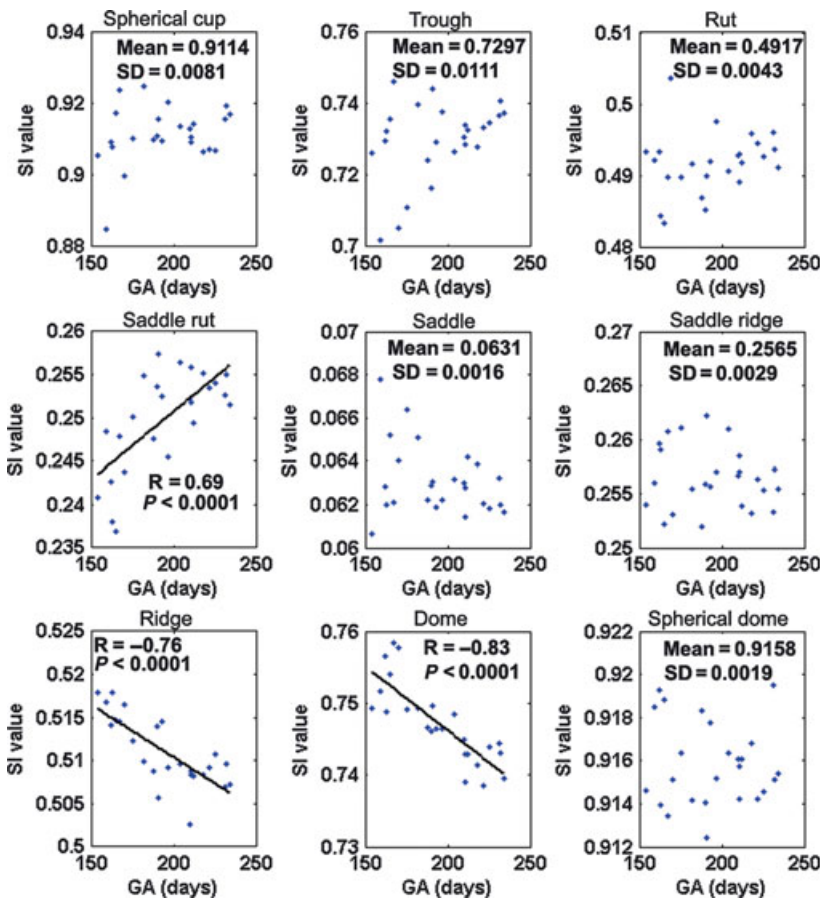

FIG. 12. Correlations between average absolute SI value and GA for nine SI scales. The ridge and dome exhibit highly negative correlation coefficients (*R*) between SI and GA, suggesting that these two shapes relate to the smoothing of the gyral surface (Fig. 9).

vary with the selected template, and does not quantify the 'real' surface shape of a surface voxel, as the SI does.

Limitations and technical remarks

Although the clinical cases recruited in this study were regarded as CNS-normal fetuses by MR examination, we cannot exclude the possibility of potential CNS abnormality.

Two advantages make the SI superior to other indices in the assessment of brain development. First, the SI value precisely reflects the true differences among cortical shapes. This characteristic overcomes the limitation of previously proposed indices. One such index, the gyrification index (GI), uses the ratio between the inner and outer cortical lengths (Zilles *et al.*, 1988). This has been extended to the surface ratio between the brain and its convex hull polygon (Rodriguez-Carranza *et al.*, 2008). This GI increases with cortical complexity, but is unable to distinguish distinct cortical shapes. For example, two shallow sulci and a single deep sulcus may produce similar GI values (Armstrong *et al.*, 1991). Another advantage of using the SI is that the SI value is invariant with respect to brain size (volume and surface area). Most of the curvature-based measures, such as the mean curvature, Gaussian curvature, and folding index (Van Essen & Drury, 1997), depend on brain surface area (Rodriguez-Carranza *et al.*, 2008). Thus, additional normalized factors have to be incorporated into the calculation of certain curvature-based indices to eliminate the surface dependence (Rodriguez-Carranza *et al.*, 2008).

Our study employed the Rousseau *et al.* (2006) approach which models fetal motion by a rigid body transformation using six degrees of freedom. A related study parameterized fetal motion by the use of a discrete cosine basis function (Kim *et al.*, 2009). One point to bear in mind is that fetal motion during MR scanning lowers the quality of image registration, which is the most critical step in the super-resolution technique (Park *et al.*, 2003). We noticed that both Rousseau *et al.* (2006) and Kim *et al.* (2009) used 3-mm-thick slices, as opposed to the 4-mm or 5-mm slices used in our study. Our result (Fig. 3B) shows the visually acceptable 3D coherent fetal brain images reconstructed, suggesting that the super-resolution technique can indentify fetal images with 4 or 5 mm of slice thickness. The Kim study had 24% (11/45) of the cases without visually acceptable reconstruction (Kim *et al.*, 2009), whereas our study had only 7% (2/27). The better performance of image reconstruction in our data is probably related to the reduction of the motion artefact, and the shortened scanning time resulting from the use of thicker MR slices.

To determine whether the intra-rater and/or inter-rater errors in slice selection affect the regional SI values, we randomly re-selected the reference slices that deviated from the original ones within ± 2 slices and re-calculated the regional SI values. This process was repeated four times to provide enough distinguishing power [power = 0.95 on the basis of the power analysis (Faul *et al.*, 2007)]. We finally employed the five datasets (one original and four repeated) in repeated-measures ANOVA to test the group difference in SI values between these datasets. We found no significant differences ($P > 0.05$) in regional SI values between the different datasets. This suggests that the intra-rater and/or inter-rater errors, within one or two slices, do not affect the results of SI values.

In summary, this study presents the regionalization in the shape of the cortical surface during the formation and deformation of primary cortical folding. This is a significant period in which structural measurement in relation to primary cortical folding has been shown to predict the outcome of brain function at birth (Dubois *et al.*, 2008a). The developing brain has been parceled according to significant anatomical landmarks, and cortical deformation has been quantified via the SI to construct a reliable model of regional shape differences. The results of this study may act as a significant reference for further comparison with fetal brain pathologies and for a longitudinal brain shape analysis from the fetal stage to childhood and adolescence.

Acknowledgements

This study was funded in part by the National Science Council (NSC-94-2314-B-075-056, NSC-95-2314-B-075-007, NSC-96-2314-B-075-005, NSC-97-2752-B-075-010-001-PAE, and NSC 99-2314-B-075-033-MY2), Taipei Veterans General Hospital (V95C1-105, V96Cl-135, V97C1-025, and V97ER1-005, and National Yang-Ming University (99A-C-B10).

Abbreviations

3D, three-dimensional; CNS, central nervous system; GA, gestational age; GI, gyrification index; MR, magnetic resonance; MRI, magnetic resonance image; NMI, normalized mutual information; SI, shape index.

References

Armstrong, E., Curtis, M., Buxhoeveden, D.P., Fregoe, C., Zilles, K., Casanova, M.F. & McCarthy, W.F. (1991) Cortical gyrification in the rhesus monkey: a test of the mechanical folding hypothesis. *Cereb. Cortex*, **1**, 426–432.

Barkovich, A.J., Ferriero, D.M., Barr, R.M., Gressens, P., Dobyns, W.B., Truwit, C.L. & Evrard, P. (1998) Microlissencephaly: a heterogeneous malformation of cortical development. *Neuropediatrics*, **29**, 113–119.

Corbett-Detig, J., Habas, P.A., Scott, J.A., Kim, K., Rajagopalan, V., McQuillen, P.S., Barkovich, A.J., Glenn, O.A. & Studholme, C. (2011) 3D global and regional patterns of human fetal subplate growth determined *in utero*. *Brain Struct. Funct.*, **215**, 255–263.

Dubois, J., Benders, M., Borradori-Tolsa, C., Cachia, A., Lazeyras, F., Ha-Vinh Leuchter, R., Sizonenko, S.V., Warfield, S.K., Mangin, J.F. & Huppi, P.S. (2008a) Primary cortical folding in the human newborn: an early marker of later functional development. *Brain*, **131**, 2028–2041.

Dubois, J., Benders, M., Cachia, A., Lazeyras, F., Ha-Vinh Leuchter, R., Sizonenko, S.V., Borradori-Tolsa, C., Mangin, J.F. & Huppi, P.S. (2008b) Mapping the early cortical folding process in the preterm newborn brain. *Cereb. Cortex*, **18**, 1444–1454.

Faul, F., Erdfelder, E., Lang, A. & Buchner, A. (2007) G*Power 3: A flexible statistical power analysis program for the social, behavioral, and biomedical sciences. *Behav. Res. Methods*, **39**, 175–191.

Garel, C. (2004) *MRI of the Fetal Brain*. Springer, Berlin, Heidelberg, New York.

Gilmore, J.H., Lin, W., Prastawa, M.W., Looney, C.B., Vetsa, Y.S.K., Knickmeyer, R.C., Evans, D.D., Smith, J.K., Hamer, R.M. & Lieberman, J.A. (2007) Regional gray matter growth, sexual dimorphism, and cerebral asymmetry in the neonatal brain. *J. Neurosci.*, **27**, 1255–1260.

Habas, P.A., Kim, K., Corbett-Detig, J.M., Rousseau, F., Glenn, O.A., Barkovich, A.J. & Studholme, C. (2010a) A spatiotemporal atlas of MR intensity, tissue probability and shape of the fetal brain with application to segmentation. *Neuroimage*, **53**, 460–470.

Habas, P.A., Kim, K., Rousseau, F., Glenn, O.A., Barkovich, A.J. & Studholme, C. (2010b) Atlas-based segmentation of developing tissues in the human brain with quantitative validation in young fetuses. *Hum. Brain Mapp.*, **31**, 1348–1358.

Hu, H.H., Guo, W.Y., Chen, H.Y., Wang, P.S., Hung, C.I., Hsieh, J.C. & Wu, Y.T. (2009) Morphological regionalization using fetal magnetic resonance images of normal developing brains. *Eur. J. Neurosci.*, **29**, 1560–1567.

Jiang, S., Xue, H., Glover, A., Rutherford, M., Rueckert, D. & Hajnal, J.V. (2007) MRI of moving subjects using multislice snapshot images with volume reconstruction (SVR): application to fetal, neonatal, and adult brain studies. *IEEE Trans. Med. Imag.*, **26**, 967–980.

Kim, K., Rousseau, F. & Studholme, C. (2009) Intersection based motion correction of multi-slice MRI for 3D *in utero* fetal brain image formation. *IEEE Trans. Med. Imag.*, **29**, 146–158.

Koenderink, J.J. & van Doorn, A.J. (1992) Surface shape and curvature scales. *Image Vis. Comput.*, **10**, 557–565.

Park, S., Park, M. & Kang, M. (2003) Super-resolution image reconstruction: a technical overview. *IEEE Signal Process. Mag.*, **20**, 21–36.

Rajagopalan, V., Scott, J., Habas, P.A., Kim, K., Corbett-Detig, J., Rousseau, F., Barkovich, A.J., Glenn, O.A. & Studholme, C. (2011) Local tissue

growth patterns underlying normal fetal human brain gyrification quantified *in utero*. *J. Neurosci.*, **31**, 2878–2887.
Rodriguez-Carranza, C.E., Mukherjee, P., Vigneron, D., Barkovich, J. & Studholme, C. (2008) A framework for *in vivo* quantification of regional brain folding in premature neonates. *Neuroimage*, **41**, 462–478.
Rousseau, F., Glenn, O.A., Iordanova, B., Rodriguez-Carranza, C., Vigneron, D.B., Barkovich, J.A. & Studholme, C. (2006) Registration-based approach for reconstruction of high-resolution *in utero* fetal MR brain images. *Acad. Radiol.*, **13**, 1072–1081.
Thirion, J.P. & Gourdon, A. (1993) *The Marching Lines Algorithm: New Results and Proofs*. Institut National de Recherche en Informatique et en Automatique, Technical Report RR-1881-1, Sophia-Antipolis Cedex, France.
Van Essen, D.C. (1997) A tension-based theory of morphogenesis and compact wiring in the central nervous system. *Nature*, **385**, 313–318.
Van Essen, D.C. & Drury, H.A. (1997) Structural and functional analyses of human cerebral cortex using a surface-based atlas. *J. Neurosci.*, **17**, 7079–7102.
White, T., Andreasen, N.C., Nopoulos, P. & Magnotta, V. (2003) Gyrification abnormalities in childhood- and adolescent-onset schizophrenia. *Biol. Psychiatry*, **54**, 418–426.
White, T., Su, S., Schmidt, M., Kao, C.Y. & Sapiro, G. (2010) The development of gyrification in childhood and adolescence. *Brain Cogn.*, **72**, 36–45.
Zilles, K., Armstrong, E., Schleicher, A. & Kretschmann, H.J. (1988) The human pattern of gyrification in the cerebral cortex. *Anat. Embryol.*, **179**, 173–179.

Appendix: Nine scales of SI

The SI value can be further partitioned into nine scales (Table 1), the midpoints or endpoints of which are mapped into the shapes presented in Fig. 7. The following describes the criteria for the selection of the shapes in Fig. 7 (Koenderink & van Doorn, 1992).

(1) Convexities and concavities are located on opposite sides of the SI value. Spherical convexity and spherical concavity are the endpoints of the SI value (any point on a sphere with $k_1 = k_2 \neq 0$). The 'spherical dome' is at SI = 1, and the 'spherical cup' is at SI = −1 (Fig. 7).

(2) Convexities and concavities appear on the area where they never connect with each other, and are always separated by the saddle-like shapes. The symmetric saddle ($k_1 = -k_2$,, the 'saddle' in Fig. 7) forms the value of SI = 0.

(3) Cylindrical shapes (SI = |0.5|) divide the convexities/concavities from the saddle-like shapes. Two cylindrical shapes in Fig. 7 are the 'ridge' at SI = 0.5 ($k_1 = 0$, $k_2 < 0$) and the 'rut' at SI = −0.5 ($k_2 = 0$, $k_1 > 0$).

(4) $|SI| < 0.5$ represents the saddle-like shapes. In addition to SI = 0 (symmetric saddle), SI = 0.25 (the 'saddle ridge' in Fig. 7) has been used to represent the intermediate shape between 'saddle' and 'ridge'. Again, SI = −0.25 (the 'saddle rut') has been used to represent the shape between 'saddle' and 'rut'.

(5) $0.5 < |SI| < 1$ represents the ellipsoidal convexities and concavities. Any shape perturbation drives spherical convexities/concavities ($|SI| = 1$) towards the cylindrical ($|SI| = 0.5$). Therefore, SI = 0.75 (the 'dome' in Fig. 7) represents the transitional shape between the 'spherical dome' and 'ridge'. Similarly, SI = −0.75 (the 'trough' in Fig. 7) represents the transitional shape between the 'spherical cup' and the 'rut'.